Sprayability and physical properties of Tuireann Energy Ltd nanofluid

Research report

Project supervisor: **Luewton L. F. Agostinho[1,4]**

Researchers: **Lynda Wamere[1,2,4], Samuel K. H. Jun[3], L.L.F. Agostinho[1,4]**

Author(s): **Lynda Wamere and Luewton L F Agostinho**

Leeuwarden, December 2019

1: NHL-Stenden university of applied sciences, Water Technology Research Group
2: University of Nairobi, Kenya
3: Tuireann Energy, Ltd, Ireland
4: Gilbert Armstrong Laboratory for Electrohydrodynamic Research

Gilbert-Armstrong Laboratory
for Electrohydrodynamic Research

NHL STENDEN
hogeschool

Index

1. Introduction

The use of fossil fuels and especially diesel fuel in engines is debated since the first signs of global climate change decades ago (Sawyer, 1972), (Hansen, 1981). Such discussion provided that several alternative ways of propulsion and fuels were proposed, but, as of today, the diesel engine still plays an important role in the global market (Fuels Europe, 2017). This discussion has also triggered new ways of improving the performance and sustainability of diesel engines. For instance, use of biodiesel mixtures (Xue, 2011), use of synthetic fuels (Verbeek, 2014), (Bassiony, 2016), and the use of water-in-diesel emulsions (Huo, 2014), (Khan, 2014), (Vellaiyan, 2016).

Regarding the use of water-in-diesel emulsions (W/D emulsions), it is known by the scientific community that the presence of water can enhance the performance of these engines and reduce some emissions, e.g. particulate matter and NO_x (Ballester, 1995), (Lif, 2006), (Chelemuge, 2012). The argued reason for this increase in performance is the occurrence of a phenomenon known as "micro-explosions" (Huo 2014). Although such claim is not unanimously accepted by the scientific community, it is described in multiple articles (Park, 2016) (Shinjo, 2014).

Some authors like Mura (2010) actually have claimed that the improvements may also be caused by changed temperatures; for example, the reduced NO_x emissions are, in some cases, attributed to this lower combustion temperature.

According to Park (2006) these micro-explosions, also called secondary atomization, is caused by the different boiling points of water and diesel. The authors claim that the rapid increase in temperature that the fuel experiences during injection, causes the dispersed water droplets to vaporize explosively and break up the diesel emulsion in smaller droplets, leading to a shorter combustion time.

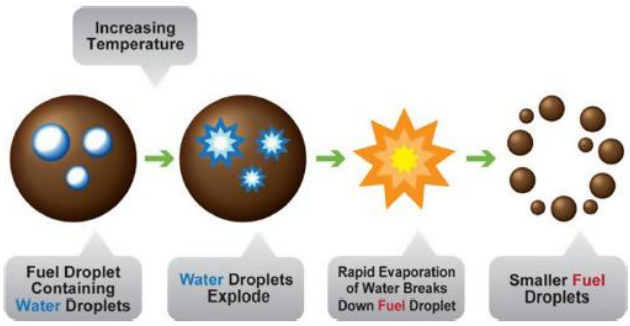

Figure 1: Micro-explosion process. (Park, 2016)

The same authors mentioned that the micro-explosion, as seen in figure 1, is the ideal situation: the water droplets are encapsulated in diesel droplets and when they break-up (explode), they break the diesel droplet into smaller droplets. Shinjo (2014) has also mentioned the so called "puffing", which is basically an incomplete breakup. According to the author, it occurs when the water droplets are not equally distributed across the diesel droplet, see figure 2 (Shinjo, 2014) (Avulapati, 2016).

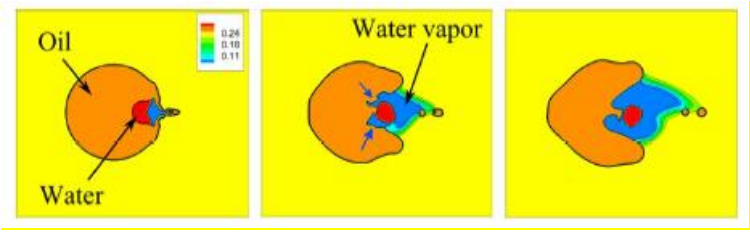

Figure 2: Example of puffing. (Shinjo, 2014)

The micro-explosion and puffing are processes, caused by the difference in several properties of water and diesel. In a W/D emulsion the water droplets are dispersed in the diesel. This emulsion is injected and also atomized into the diesel cylinder at the last stage of the compression. At this stage of the diesel engine cycle the pressure in the cylinder is increased drastically (up to 100 bar) and thus also the temperature (500-900˚C) of the air inside it (Ashgriz, 2011). This process superheats the water in diesel emulsion which will bring the water droplets to temperatures beyond their boiling point but stay in the liquid phase. When the droplet is then disturbed by external forces, e.g. vibrations, it explodes violently and the diesel brakes up into smaller droplets, all happening in matters of milliseconds (Namioka, 2012), (Mura, 2010). These smaller droplets have a higher surface area where vaporization takes place and thus the droplet vaporizes faster. The faster vaporization is also one of the reasons why less particulate matter is found in W/D emulsions, because the fuel is combusted completely before the pressure and temperature are dropped to a point where incomplete combustion takes place (Ogunkoya, 2015).

Contrary to most exposed theories, Ashgriz (2011) mentioned that micro-explosions probably do not occur in diesel engines because the atomized diesel droplets (in the cylinder) are too small (1-10 µm) to contain a sufficient amount of water droplets in its volume. However, it appears to be no consensus in the literature regarding the expected/ideal size of the injected diesel droplets in their respective engines as the authors have found different sources (mostly internet links) claiming sizes between 10 and 400µm.

There is also some literature available regarding the insertion of nanoparticles to enhance the performance of such engines. In this line the review presented by Saxena et al (2017) is a good collection of all the different efforts done to improve the efficiency of such engines using (organic, inorganic, colloidal) nanoparticles.

The effectiveness in performance of manganese oxide and copper(II) oxide as additives in diesel engines were compared by Lenin *et al,* 2013. Manganese oxide was observed to be the more effective among the two. However, particles of the additives could be found in inhalable particles. Guru (2002) studied exhaust gas contents after using manganese, magnesium, copper and calcium as fuel additives. Manganese showed a stronger effect in improved combustion efficiency, since the cetane number was observed to increase with an increase in dosage of additive, i.e. better combustion of the fuel in the engine.

However, two important aspects have to be considered (and deserve more investigation) in such implementations, namely: (i) the ratio between the inserted (nano)particle (or, in the case of water and diesel emulsions, water) and the carrier, and (ii) the most appropriated atomization method to bring these particles (liquids) to the combustion chamber.

In the work presented by Bos (2017), the author mentioned as well, that there appears to be no consensus about a defined/ideal size for diesel droplets atomized in the combustion engine. However, as mentioned above, sizes between 10µm and 400µm are reported. In his report, Bos has decided to target 20µm given the difficulty to obtain uniform size droplets of this size. Whenever these droplets will have to be encapsulated or not, i.e. with water or nanoparticles, in the case of diesel and water solutions, this size has to be considered to avoid incompatibilities between the agent size and the carrier. The same applies to nanoparticles additives. In that case, the size of the droplets might vary, from what was published by Bos, to guarantee ideal performance, but, whenever chamber size and total explosion volume is considered, the average size should remain around the same range. Thus, if one considers that liquid carriers would have to sustain such diameter, the added solid (or emulsified agent) would have to be much smaller. Additionally, and, to the best knowledge of the authors not well described in the literature yet, this relation between size and total presence/concentration of

these agents in the carriers itself is not extensive disclosed, both for nanoparticles and for emulsion-based products.

In this research electrohydrodynamic atomization (EHDA), also known as electrospray, is proposed as a possible method to analyze the behavior of droplets from a defined nanofluid regarding size, size dispersion and electric charge. EHDA is a technology based on the breakup of a liquid, pushed through a capillary nozzle under the influence of a strong electrical field ($kV \cdot cm^{-1}$). It is already used in a wide variety of applications namely: drug encapsulation (Pareta, 2006), bio-encapsulation (Wu, 2008), thin film coatings (Sridhar, 2013), and more recently to atomize biocides in greenhouses (Agostinho L. L., 2014). Some advantages of this technology, over other atomization methods, is that it allows a good control of the produced droplet size (down to ηm range), it can generate narrow size distributions, and it uses comparatively low amounts of energy (Grace, 1994), (Sadri, 2012), (Agostinho, 2013). Castillo-Orozco *et al* (2017).

In the specific case of this work, via controlling the droplet size with EHDA, it could be inferred whether the nanoparticle size would eventually interfere in the droplet formation mechanism. Additionally, some assumptions could be made regarding the nanoparticle density per droplets, and, via electric charge values, how/if such particles could interfere in the droplet surface charge, i.e. surface charge can be used as a droplet trajectory mechanism.

To be able to optimize the EHDA tests, the nanofluids were characterized regarding particle size, surface tension, permittivity, density, electric conductivity and viscosity. Additionally, to facilitate some assumptions regarding the particle distribution inside the liquid, extra solid analysis, zeta potentials tests and bacteria growth tests were performed.

2. Materials and Methods

The tests performed in this work were done in bench (lab) scale. The text presented below describe the setup and method used for the tests.

2.1 – Characterization of the samples

In this phase of the experiments we characterized the fluids made available by Tuireann with two specific objectives: (i) optimize the EHDA tests and (ii) better understand the (nano)particle size and size distribution.

The company has provided 3 different fluids which will be, from this point of the report onwards named as T1D, T1F and T2. Mainly, the differences between T1D and T1F is the sample preparation time. Being T1D older than T1F the most recent. T1 samples and T2 samples differs from each other in the total solvent content. As the specific characteristics of each fluid is not the object of this research, they will not be described in more details.

The samples were characterized regarding their surface tension (Kruss Tensiometer K6), electric permittivity (hp 4194A impedance/gain-phase analyzer with a BDS novocontrol sample holder), density (analytical method), electric conductivity (Hach EC probe) and viscosity (rheocompass 1.19).

Additionally, each sample was also characterized regarding the particle size (DIPA 2000 particle size analyzer). The method is applicable for micrometer size range, especially for sizes between 5µm and

300µm. Thus, nanometer size particles will not be detected and therefore counted. As many different mechanisms could lead to formation of particles (clusters) bigger than 100µm, and the literature reports droplet size targets between 10µm and 400µm, few particle size tests (as well atomization tests) were conducted with the raw samples and after filtering them through 10µm and a 2µm filters.

Extra tests were done as well to verify metal content (ICP EOS analysis). In these tests the presence of Al, Cr, Fe and Ni was evaluated, i.e. the metals were requested by the company and are expected to be either the constituents of the nanoparticles or originated from electrochemical reactions used to produce them. Additionally, also using ICP, the total Na content was evaluated.

In a later phase of the experiments, the particle size analysis indicated the presence of particles bigger than the filter porous, after filtration, in some samples. To evaluate the reason of such results the samples were tested regarding the presence of bacteria, i.e. it is known in membrane filtration systems that some bacteria can change cellular shape to be able to pass through filter porous much smaller than their steady condition diameter (Hasegawa *et al* 2003), as well as regarding agglomeration using TSS content in the filter (weighing method).

Lastly, zeta potential analysis of the samples was performed in order to verify the nature of solvated charge inside the liquid.

2.2 – EHDA Sprayability

The EHDA sprayability tests were conducted mainly to verify the charging aspect of the produced droplets compared to a NaCl+Water solution with similar Na concentration (as found in T1) and to tap water. Additionally, the tests also investigated the relation between the used flow rate and electric potential to produce a specific droplet size/population, i.e. between 10 and 400µm. Even though, in the specific case of Tuireann, the fluid is expected to act as an additive and the droplet size for improved (best) performance is rather variable and yet unknown.

The tests were conducted with a nozzle to plate setup (see figure 3). The nozzle used for the tests were the Nordson EFD precision nozzle (red gauge, 7018333, 7018345, 7018366, ID = 0.25 mm and OD = 0.52 mm). The distance between nozzle and plate was 2cm. In all experiments the high voltage was applied to the nozzle (holder), while the plate was kept at ground. To be able to observe the electrospray modes, quantify the droplets and characterize them, a high-speed imaging setup was used. This high speed imaging setup consisted of a high-speed camera (Photron AS2), with back light illumination (Dedo Cool Light) and a microscopic lens (Navitar 125x). During the tests the system was also used to verify the spray mode. After acquired, the images were analyzed with ImageJ®.

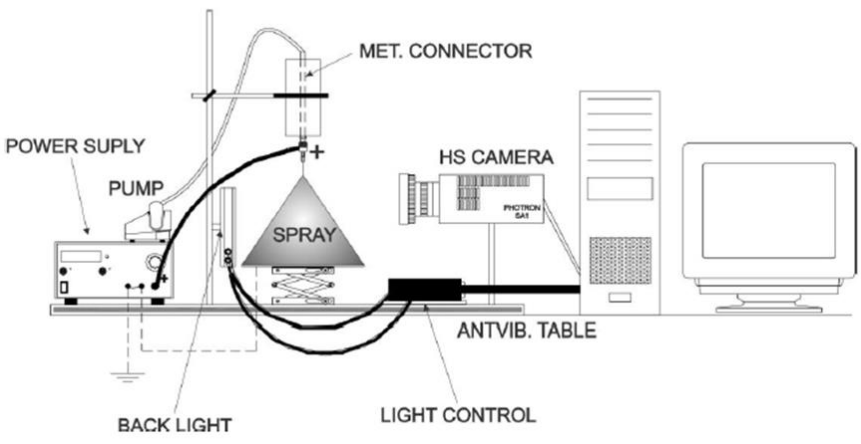

Figure 3- EHDA setup used to characterize the droplets and spray.

The spray tests were conducted in the following way. For each fluid the Weber number (see Agostinho, 2013, PhD thesis) was calculated to define which flows would provide a We < 1, and, thus, provide that the spray would be operating in the dripping regime. From the calculations, the following tests flows were defined: 5, 10, 15 and 20 $mL.h^{-1}$. For each flow, the electric potential was varied between 0 and 9kV (multi-jet mode) in steps of 1kV, i.e. few tests done with T1 were conducted at higher potentials, i.e. between 10 and 13kV. These tests allowed the definition of the EHDA mode window, i.e. for each flow, which potential will trigger the different modes. The EHDA mode definition was done using the diagram presented by Agostinho et al 2018, also represented in figure 4.

From the diagram, it is possible to see that, inside the dripping regime, the EHDA modes differ according to the applied potential. During the experiments, it was observed that the dripping, micro dripping, intermittent cone-jet mode and multi-jet mode could be achieved. Due to the high surface tension of the liquid, cone-jet mode was not seen.

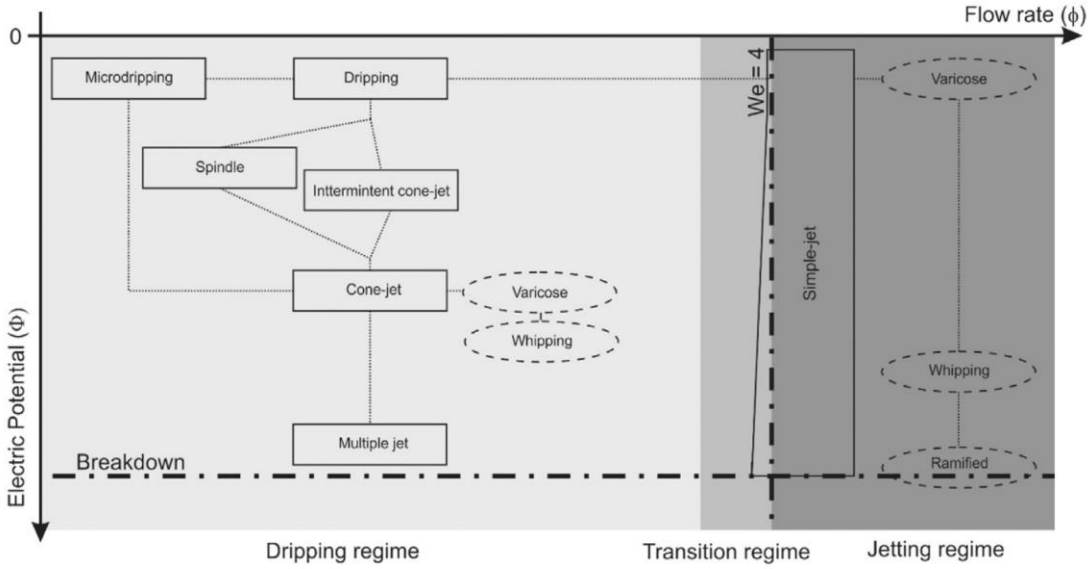

Figure 4: EHDA mode diagram as defined by Agostinho et al (2018) in the special edition of the Journal of Aerosol Sciences.

During the spray tests, the electric current was monitored to allow an estimation of the droplet charge. This monitoring was done connecting a portable multi-meter (U1233A model) to the ground line. This estimation was done by assuming that the total spray charge was equally distributed to all the produced droplets. As the high-speed image movies allows a good estimation of the total amount of droplets produced per time unit, such method is a straightforward way to estimate droplets charge. However, given the low level of the current in EHDA, it is expected that some errors are incorporated via this measurement. During these tests a solution of 2.5g/L of NaCl was also prepared, with a similar ion content as obtained with T2, to verify whether the charge level with monovalent ions salt solution would be comparable to those obtained with the fluids.

3. Obtained Results and Discussion

The current section will present the obtained results and provide discussion about them. The presentation of the results will follow the same structure as presented in the method section.

3.1 – Characterization of the samples

The table presented below (table 1) is a summarized representation of some data obtained from the characterization of the samples, i.e. density, conductivity, viscosity and surface tension. As it can be seen, two other solutions are included in the results, water (which will be used as a reference solution) and a 2,5 g/L water and NaCl solution which will be used to infer about the role of the metal particles on droplet charge. The concentration was selected because it represents the expected concentration of sodium in the T1 and T2 samples.

Table 1: Physical characterization of the fluids, water and NaCl solution (2.5g/L).

Parameter	Sample				
	T1D	**T1F**	**T2**	**NaCl**	**Water**
Density, kg/m^3 (± 2.3)	1001	1001	986,5	1002.5	1000
Conductivity, mS/cm (± 1.2)	11,8	11	6,4	5,3	1,2
Surface tension, mN/m (±1.6)	65,5	63,0 ±	55,0 ±	74,0 ±	72,6
Viscosity, Pa.s (10^{-3} at 25oC)	0,9	0,9	0,88	0,92	1

From the analysis, it is possible to observe that the obtained values for the tested fluids showed some similar density when compared to the reference solutions, i.e. water and NaCl. Except for the T2 fluid which showed slightly lower densities (1.4% lower). As the chosen spray configuration is vertical, lower gravity could play a role on requiring slightly higher potentials to provide the same spray mode, for such small differences, it is, nevertheless, not expected to be an observable influence. The lower surface tension (compared to water) indicate that capillary forces (between the liquids and the nozzle surface) will be also lower, thus, smaller droplets can be formed with lower potentials. However, the values found are still quite high, thus would still require strong electric fields to reach more stable modes, i.e. the cone-jet mode. This is confirmed by the experiments, as a stable cone-jet mode could not be achieved within the experimental conditions.

High conductivity levels (K) indicate more presence of available (mobile) ions (compared to water). To better understand the relation between permittivity and frequency, a plot is presented in figure 5.

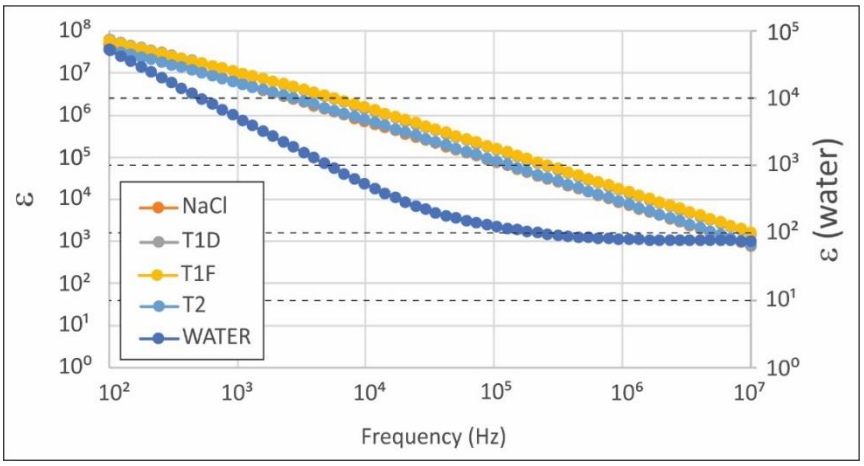

Figure 5: Relative permittivity versus applied frequency for the tested fluids. As the values found for water were relatively lower when compared to other liquids, the Y axis for this specific liquid is represented on the right side of the plot (secondary axis). To facilitated visualization, all the axis are presented in logarithm scale.

It is possible to observe, from figure 5, that the tested liquids present relative permittivity in the same range as measured for the NaCl solution, and around three orders of magnitude higher than the values measured for water. It is important to observe that the frequency range used for the experiments is between 100Hz and 10MHz (equipment limitation). In this frequency zone, the process that influence the response of the tested liquids to the variable field is mostly ionic. In the MHz zone dipolar relaxation starts to play a role as well. In this zone it is also expected that the permittivity values would be rather high, i.e. seen in the values found both for the NaCl solution and the tested (T1 and T2) solutions. Water has a rather constant relative permittivity between 1MHz and 1GHz, thus the values found in this range would be compatible with values found in the literature (normally expressed for 20MHz).

The high values observed for the tested fluids, when compared to water, are probably caused by the presence of the (metal) nanoparticles, which create molecules clusters, which decrease the response of the fluid to the field, i.e. as done by the NaCl ions. However, further investigations have to be conducted to confirm such hypothesis.

If water is excluded from the plot, the relation between the tested fluids and NaCl solution is better visualized. Figure 6 presents this relation for frequencies between 100Hz and 10kHz.

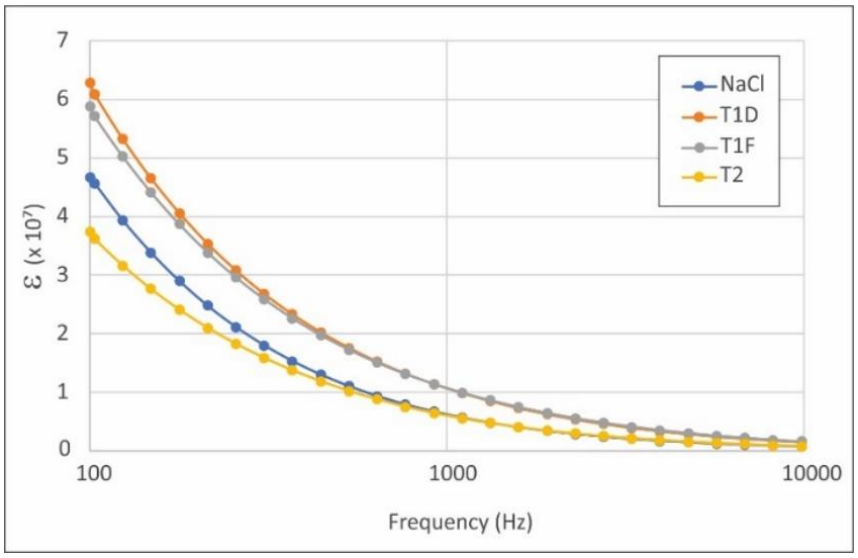

Figure 6: Relative permittivity versus applied frequency (Log) for the tested fluids and NaCl solution between 100Hz and 10kHz.

As it can be seen, T1D and T1F, as expected, have quite similar behaviour and present, for the frequency range below 1kHz, higher permittivity than the NaCl solution. Within the same range (below 1kHz), T2 presents lower permittivity and above that, similar permittivity than that measured for the NaCl solution. Above 10kHz, all the substances present very similar relative permittivity. Such results basically attest that T2 has a higher ionic mobility than the tested NaCl solution for low frequency fields (quasi static environment) whether T1 is lower.

Another observed aspect (figure 7) was the fact that, especially for T1, and for frequencies in the MHz range, negative values of the real permittivity (ε') were found. For T2 ε' values were all positive, with some few exceptions found in few samples (each liquid was measured at least 4 times) for the last (high frequency) values, i.e. above 4MHz (not shown in the plots).

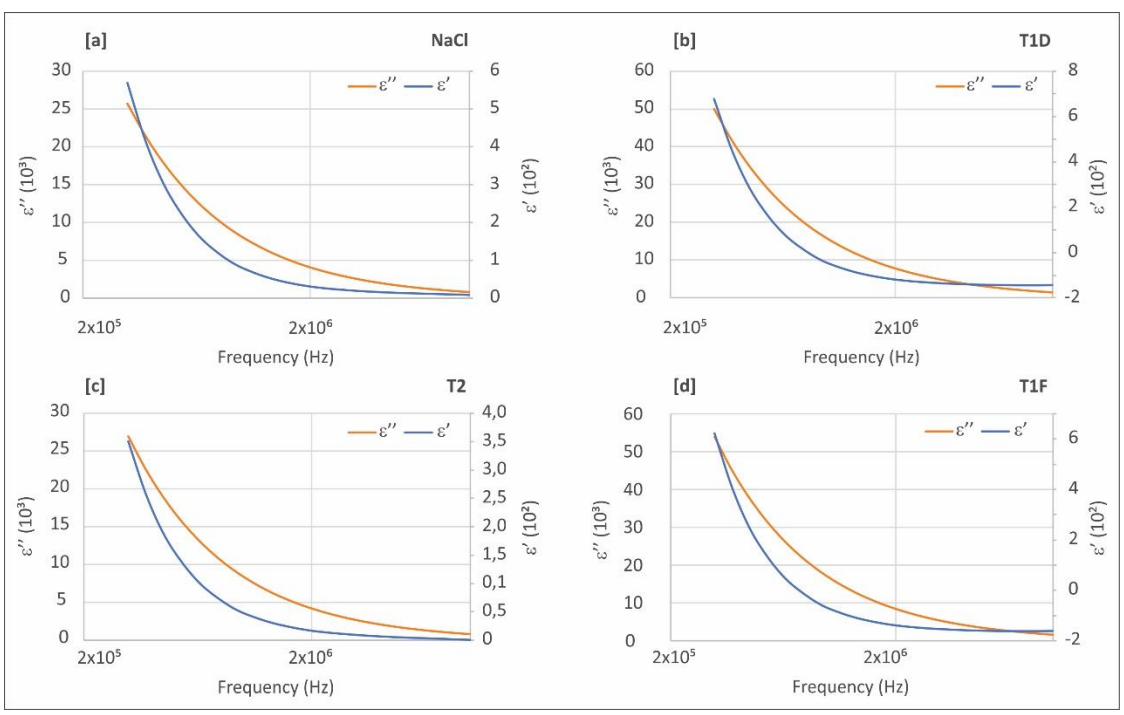

Figure 7: Real (ε') and imaginary (ε'') permittivity values for NaCl (7a), T1D(7b), T1F(7c) and T2(7d) in the frequency range between 0.2Mhz and 10MHz.

Negative real permittivity values of water are already reported in the literature by Cherpak et al (2003). The author discussed that such inversion of the real permittivity vector is observed in the interface between the water molecules and a solid-adjacent layer (the authors used Teflon in their experiments). A similar phenomenon was extensively discussed in the literature by the group of G. Pollak, when also investigating the behaviour of water molecules (and many other polar solvents) in the interface between the liquid and adjacent-solids (Pollak et al 2010). It is important, however, to mention that the tests performed in this research were not focused on defining the permittivity at (or close to) a very specific interface, rather on the permittivity properties of the liquid itself. However, the test cuvette used by the equipment utilized to perform the tests is a Teflon cuvette with top and bottom golden electrodes. This could justify the negative values found for the real permittivity (using Pollak and Cherpak approach), however, in that case, such negative values should be also found for the measurements done with Water and NaCl, which was not the case. Such findings indicate, thus, that the tested liquid have a different real permittivity behaviour when compared to water and the tested NaCl solution, in frequencies around the MHz range. More investigations need to be performed to better understand this behaviour. Finally, it is also recommended that extra tests should be conducted with higher frequencies (GHz range). As the negative values were specially found for higher frequencies.

Another investigation conducted was the calculation of the ratio between the liquid electric permittivity (ε) and its conductivity (K), known as the electric relaxation time (Hartman, 2003) represented in equation 01 below.

$$\tau = \frac{\varepsilon_0 . \varepsilon_r}{K} \qquad \text{(equation 01)}$$

In the case of the tested liquids, permittivity was measured in a range of frequencies (as shown in Figure 8) and conductivity was done for quasi-static (electric field) situation. Therefore, the calculations done to determine the substance's electric relaxation time were conducted using a constant conductivity (values expressed on table 01) and the permittivity values within the evaluated frequency range.

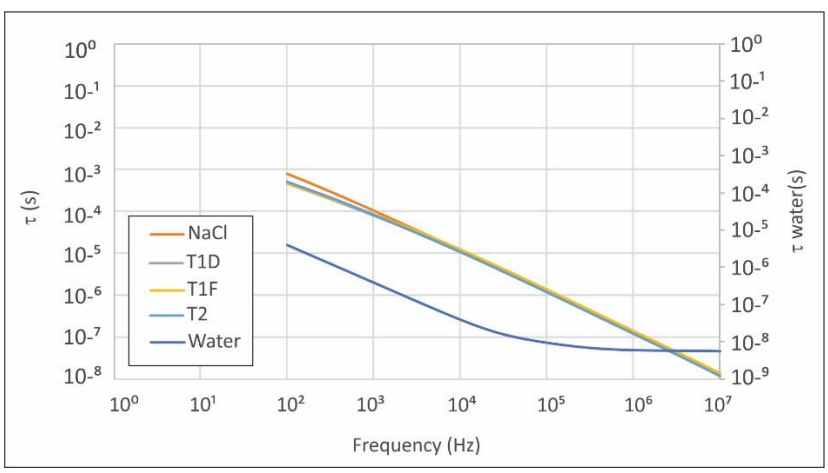

Figure 8: Calculated electric relaxation time for a constant conductivity within 100Hz and 10MHz. The values found for water are plotted as a secondary axis to facilitate comparison.

The values found indicate that the liquids present relaxation time in the order of miliseconds (100Hz) to few tenths of nanoseconds (MHz), i.e. water, as also seen in the picture, has relaxation time in the order of micro (100Hz) till tenth of nanoseconds (10MHz). A direct consequence of longer relaxation time (specially found for lower frequencies) is that the liquid will take more time to build surface charges, but, in consequence, it will also carry the built-up charge longer (slow relaxation). In the case of atomized droplets, one could conclude that, when sprayed in the same continuous phase (air, vacuum, water), the T1 and T2 droplets will hold their surface charge for longer periods.

Lastly, if considered that the permittivity is more related to dipole orientation than to ion migration (contrary to conductivity which is intrinsically linked to ion migration), it can be concluded from the analysis as well that the presence of the nanoparticles affects both dipole orientation and charge migration, however it has a stronger effect on charge migration, when compared to water.

3.1.1 – Analysis of cation(s) concentration in the fluids

ICP analysis were also performed to verify the presence of different cations in the fluids. As mentioned above, these tests were conducted to quantify the concentration of Fe, Ni, Al, Na and Cr. The cations were selected based on the composition of the fluids provided by the company. The results are shown in sequence.

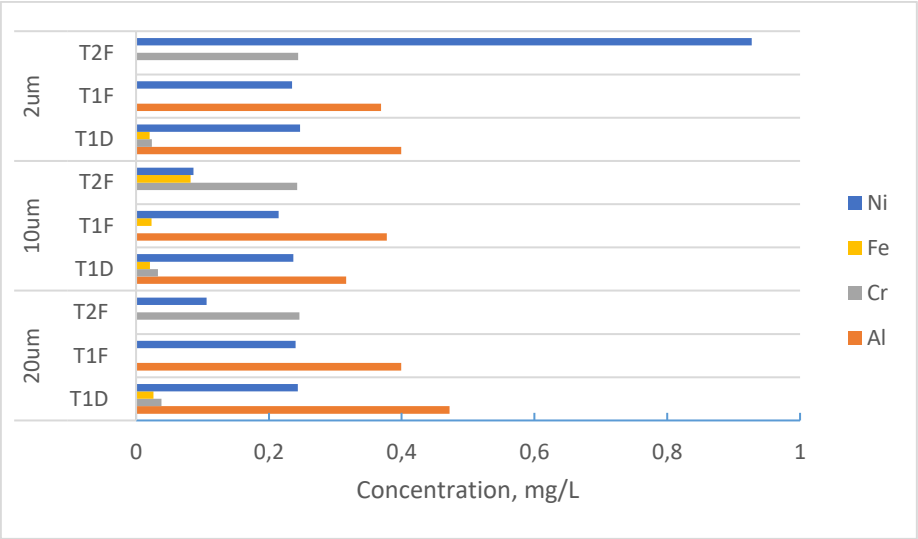

Figure 9: ICP analysis of main cations present in the tested fluids.

From the ICP analysis it is possible to observe that the metal concentrations are below 1 mg/L. Also the most present ions are Ni and Fe, even though their concentration change according to the tested fluid. The results show that, as expected, the filters are not removing the cations as they are found in similar concentrations before and after filtration. Ni is present in all solutions but for T1F (also not encountered in unfiltered). Aluminum was found to be present only in T1 solutions and, apparently, its total concentration might be affected with the time the solution was prepared (concentration T1D < T1F). With exception of results found after filter 10um, which indicates slightly higher values in T1F when compared to T1D. Chromium was found in all fluids but for T1F. Iron was consistently present in T1D but not found in the other fluids. With exception of some traces found in T2F after 10um. However, the fact that the metal was not found in T2F unfiltered, indicates a probable contamination.

Figure 10 shows the results obtained when the concentration of sodium was examined in the different fluids.

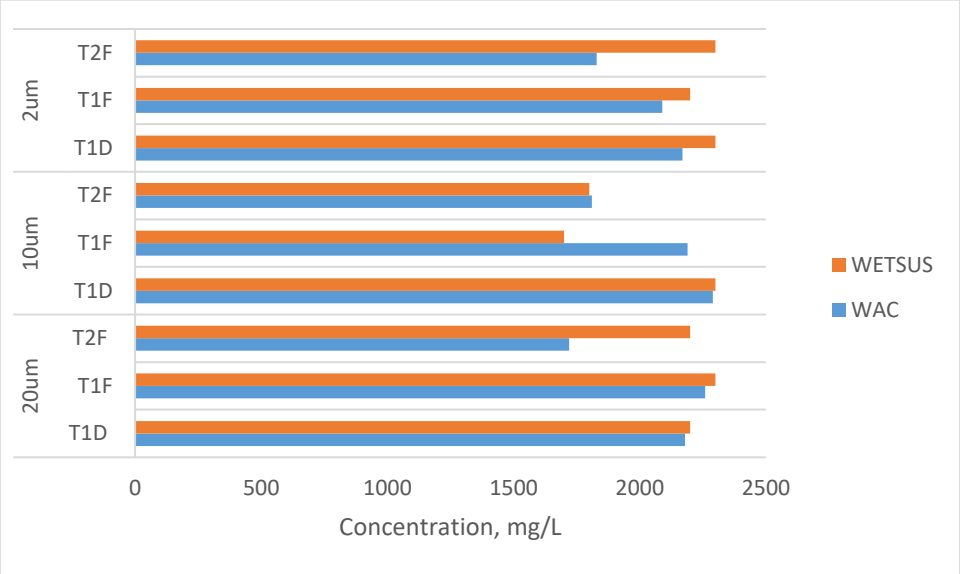

Figure 10: Concentration of sodium on the tested fluids.

For higher accuracy the Na tests were conducted in two different laboratories (WAC and Wetsus). The overall conclusion from the plots, is that the sodium concentration is, in average, 2,5 g/L for all the tested samples.

3.1.2 - Particle size analysis (DIPA 2000)

The fluids were also analyzed regarding particle size. The results are shown in figure 11.

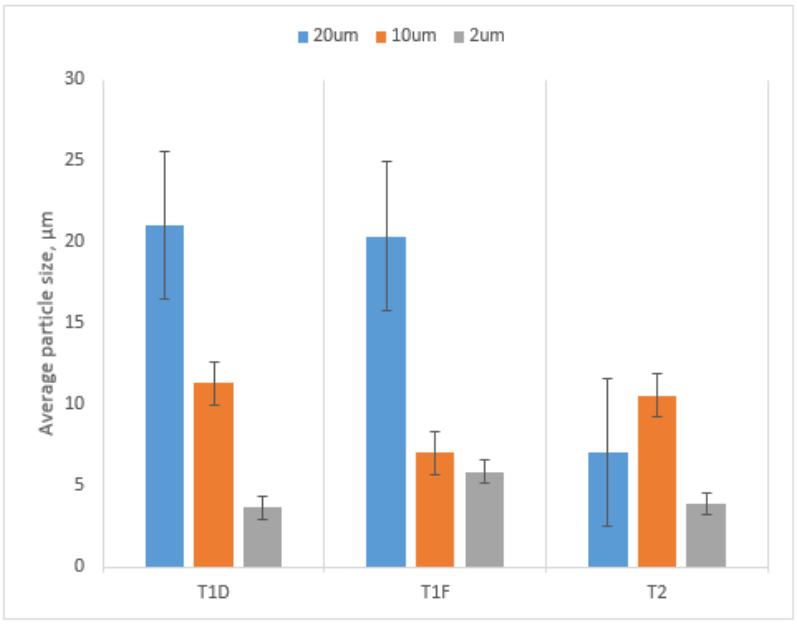

Figure 11: Particle size analysis for the different fluids. The column value is the particle average size, the error bars are the measurement standard deviation. Particle concentration found for all the samples range between 10^3 till 10^4 counts/mL. As the tested volume is 100mL, in multiple runs, the

total particle count is in the range of 10^5 and 10^6 particles per sample. More specific details about number per samples can be found in the attached documents (particle size analysis).

As it can be seen, the average particle size encountered in all the tested fluids ranges between 3.7 and 20.4 µm. The plot also shows, as expected, that the filtration steps in T1 decreases considerably the particle average size. The errors represent the standard deviation of each measurement, which allow the conclusion that the data was not highly dispersed.

Some conclusions can be made from these results. First one is that there is no apparent effect of the sample aging (not within the period between two samples tested in this work) on the average particle size, as it can be seen that the average size of T1D and T1F (20 µm) fluids are comparable. Conversely, particle size for T2 (20 µm) is significantly smaller than T1. This is attributed to the preparation process of sample T2, which comprises a filtration step done with a 10 µm pore sized filter (information provided by the company).

Also, the results show the presence of (few) particles still bigger than the filter porous size. Such effect, nevertheless, can be attributed to the equipment accuracy (the analyser used has better accuracy for particles bigger than 5µm), agglomeration of the particles after filtration as observed in alumina nano particles (Ilyas et al., 2016) and lastly, but less probable, bacteria that can change shape to pass through the filter pores (Gaveau et al., 2017).

Lastly, it can be inferred that, if the target is the production of droplets in the 10-20µm size, when one considers that the particle sizes encountered in the non-filtered fluids are above that size, the solutions have to be filtered with 2um filters or smaller. As it can be seen, considering the equipment error and size dispersion, after the 2µm filters, the particles get diameter in the order of 3 -5µm, which would allow presence of around 60 particles per droplet (of 20µm). It has to be mentioned that the ideal number of nanoparticles per droplet to guarantee an ideal efficiency of the fluids, it is not yet known. However, with EHDA, it is possible to tune such value by controlling the particle size and droplets size as demonstrated in this short test.

More detail about the particle size analysis for all the fluids can be seen in annex documentation (folder named “particle size analysis”) and in a separate Excel folder named “particle sizes”. Where all the histograms obtained by the analysis are shown.

3.1.3 – Microbiological analysis of the fluids

During the experiments, suspended material was seen in some samples. After discussion with the company, it was mentioned that such material could be bacterial growth, i.e. specially because the samples which presented such material were those prepared first (old samples). To verify such assumptions, the samples were analysed regarding total bacteria content.

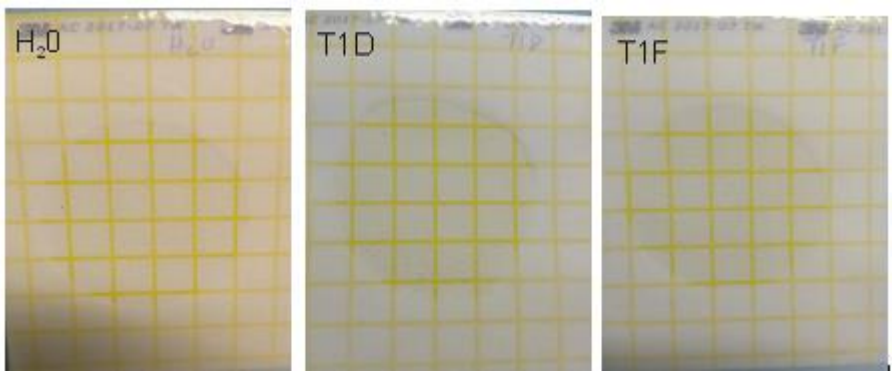

Figure 12: Bacteria tests in the fluids

The test was a simple test of colony growth in agar media. The presence of bacteria is indicated by the formation of colonies in the media (represented by small red dots). As it can be seen, the sample T1D and T1F were comparable to the control test (deionized water).

3.1.4 – Sprayability

To check the (EHDA) sprayability the liquid is first tested regarding the relation between flow rate and potential to achieve different EHDA modes. In such test, each one of the experimented flow rates (see method section) are subjected to different potential levels and the potential windows which allow the formation of the different electrospray modes are defined. As the liquid properties do not change during the test (just the flow rate and potential), and the selected flows are all inside the dripping regime (We < 1), the achievable modes are expected to be the same, just at different potential window dictated by each tested flow rate. In the fluids tested, the following modes were observed: dripping (zero potential), fast dripping or electro-dripping, intermittent cone-jet mode (with straight breakup and with alternating lateral break-up). Given the high surface tension of the fluids, the cone-jet mode was not achievable.

The tests were done to verify the influence of the flow rate, electric potential, liquid type and filtering method on the droplet size and size dispersion. As mentioned above, the smallest droplet size targeted was 10µm (average size). The size distribution of the droplet population was evaluated using the Relative Standard Deviation (RSD), which, according to the literature (Agostinho, 2012), is an indication of monodispersity whenever below 0.2.

Also, the liquid flow rates were defined in order to provide flows for average combustion engine consumption, i.e. 10-20 L/km, even knowing the main intention of the fluids is to be used as an additive, not as main fuel. Thus tested flows are higher than eventually needed. But, as main challenge of EHDA is to work in high flow conditions, i.e. at high flows droplet diameter is intrinsically related to nozzle diameter, producing droplets of required size for these high flows, would mean that such target can also be achieved for lower flow rates.

The figure below is a representation of all the EHDA modes observed during the experiment for all the tested fluid.

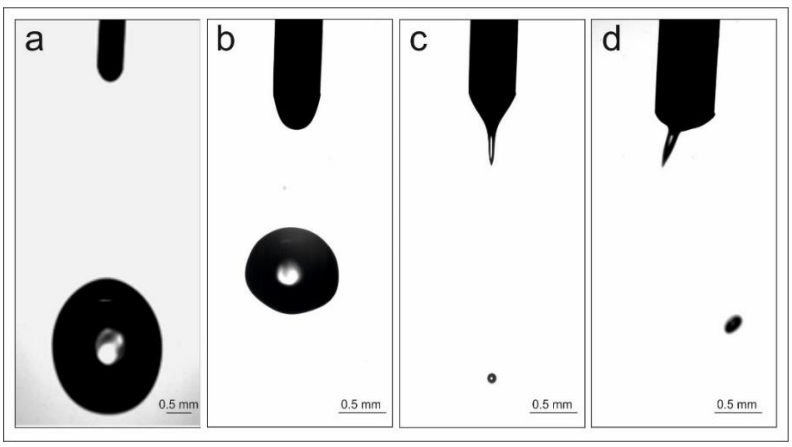

Figure 13: Different EHDA modes obtained during the tests. Figure 13a is the dripping mode (no potential applied). Figure 13b is the micro dripping mode. Figure 13c and 13d are the intermittent cone-jet mode with straight breakup (13c) and lateral breakup (13d). The modes are obtained, for

the different flows, with different potential values, but the potential from 13a to 13d is, in all cases, increasing.

In resume, in the experiments all the modes inside the dripping regime before the cone-jet mode were achieved, i.e. as mentioned above the high surface tension of the liquid did not allow achieving cone-jet in ambient conditions. As it can be seen in figure 13a in the dripping mode (no potential applied) the droplets are few times bigger than the nozzle diameter. As soon as the potential is applied, the micro-dripping mode is achieved, allowing the formation of droplets still bigger than the nozzle diameter, but smaller than those obtained in the dripping mode. For even higher potentials, the spherical meniscus is changed into a conical meniscus which relaxes back every now and then forming a droplet in the process, this is the intermittent cone-jet mode. In this mode the formed droplets are smaller than the nozzle diameter, as it can be seen in figures 13c and 13d. In our experiments we have seen the intermittent cone-jet mode with straight break-up (figure 13c) and, for higher potentials, the intermittent cone-jet mode with lateral break-up (figure 13d). As it will be seen in the data presented in sequence, the average droplet size between intermittent cone-jet with straight break-up and lateral break-up is not very different. However, the spray pattern changes quite significantly producing sprays which occupies better the volume of the chamber.

Figure 14, presented below, are different stacks done when multiples images of the same spray are super imposed. In the figure is possible to see that, the size dispersion in the intermittent cone-jet with straight breakup (figure 14a and 14b) is quite narrow (droplets of very similar size). Whereas, for the lateral breakup (figures 14c and 14d), it is rather broad. Also, the pictures show that the spray angle for lateral breakup is much bigger. Considering that a broad dispersion of the sprayed droplets inside the evaporation chamber would allow better convection and, therefore, enhance evaporation, such large spray angle can be seen as an advantage.

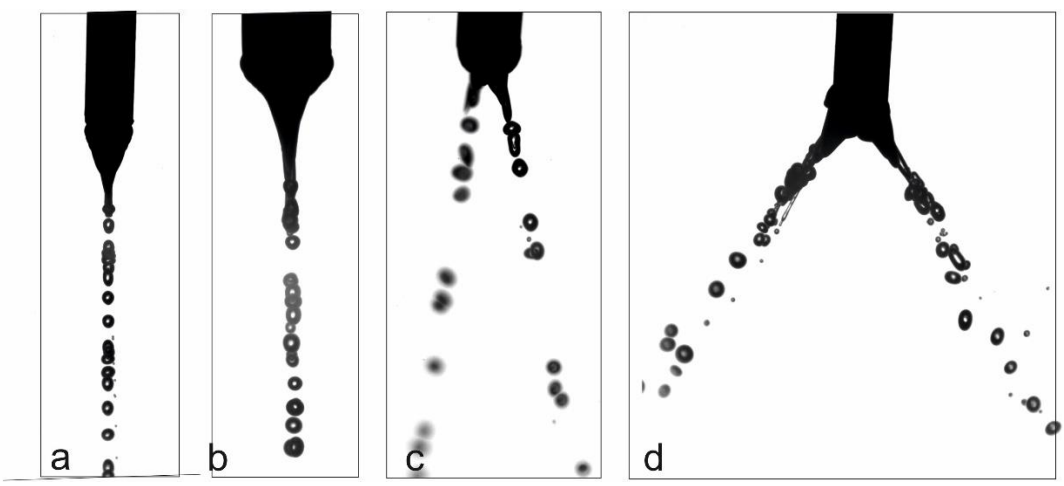

Figure 14: Superimposition of images of the same spray. The images are a representation of the droplets produced by different sprays being: T2 5mL.h^{-1} 4.5kV after 2µm filtration (14a) T1O 5mL.h^{-1} 4.5kV after 2µm filtration (14b), T1F 10mL.h^{-1} 6.0kV after 2µm filtration (14c) and T1D T1F 15mL.h^{-1} 6.0kV 20µm (14d).

In the next section the influence of the applied flow rate, the electric potential, the filter size and type of fluid on the droplet size and size dispersion will be explored. A more complete table presenting the electric potential necessary to stablish the different modes with the different fluids after and before filtration, is presented in annex I.

3.1.4.1 – Influence of the applied potential on droplet size and size dispersion

Figure 15 presented below is a representation of the droplet population generated for T1D after 2µm filtration operating at 15 $mL.h^{-1}$ with three different potentials, e.g. 4.5, 5.5. and 6.5 kV. At the first and second potentials the spray is operating in the intermittent cone-jet mode with straight breakup and at 6.5kV with lateral breakup. Due to the low droplet production ratio, the droplet populations produced in the dripping mode (Pot = 0) and enhanced dripping (Pot < 4.5kV) is not shown.

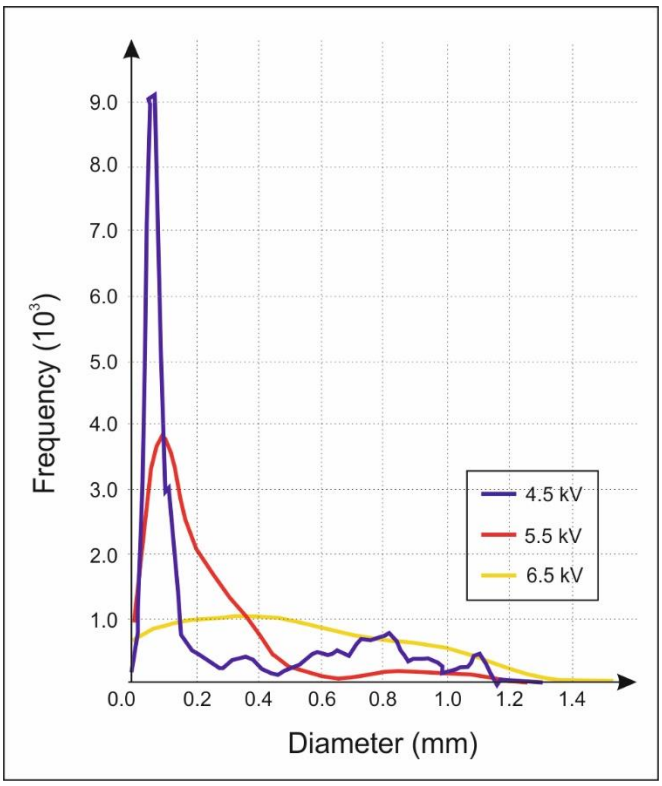

Figure 15: Droplet populations produced with T1D after 2µm filtration.

From picture 15 it is possible to see that the average droplet diameter in the straight breakup are 180 and 100µm, for 4.5 and 5.5kV respectively. For the highest potential, 6.5, the population gets much broader dispersion, with droplet average size of 450µm. The data also show that, inside the straight breakup window (4.5 and 5.5 kV) the higher the electric potential the narrower the population is. This is also expected for sprays operating with such liquids as reported by Agostinho, 2013, for EHDA in the simple jet mode. Another important information from the plot is that, the smallest droplet size targeted, i.e. 10µm, could not be achieved with the experimented setup and configuration. This is basically caused by two reasons (i) the chosen nozzle diameter, i.e. 210µm, and the potential window (< 7kV). To verify such assumption new tests were performed with T1 (only) using a smaller nozzle (gauge 32, EFD precision, ID=0,10mm OD=0,24mm) and higher potentials. The results are shown in figure 16.

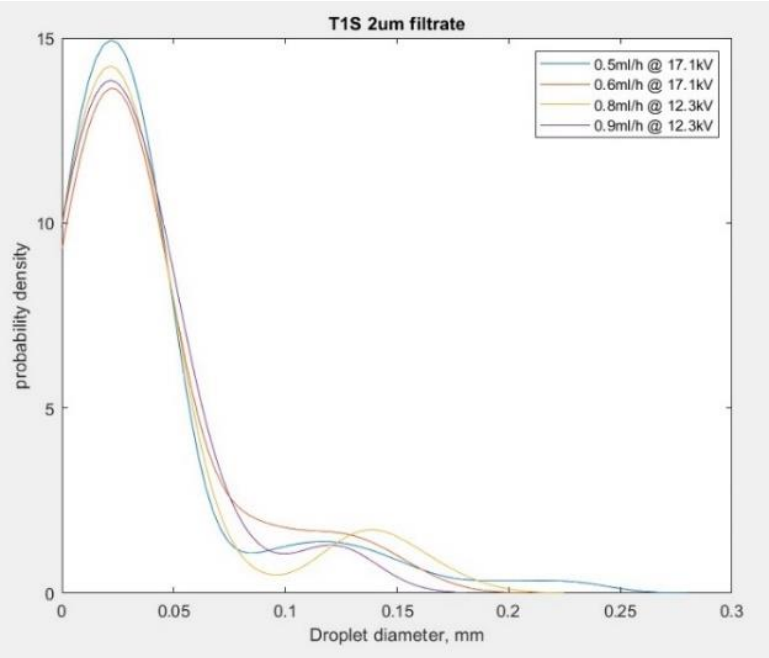

Figure 16: Droplet size distribution for different flows and different potentials using T1 and smaller nozzles (gauge 32).

As it can be seen, in that case, the average droplet size was ~25µm with a large part of the population between 5µm (optical limit of the imaging system) and 25µm. In this experiment the potentials used were quite high (around 12kV), which, in practice, would bring some instability to the system due to corona wind and possible sparks. This was seen during the experiments as well. More stability can be achieved, however, using a more inert gas as continuous media, i.e. CO_2.

3.1.4.2 – Influence of the applied filter on droplet size

When the influence of the applied filter is observed, it can be mentioned that the finer filters do impact the droplet formation for the tested flows and potentials. Figure 17 presented below is a representation of such effect for fluid T1F with experiments done for different potentials and using a flow rate of 15 $mL.h^{-1}$.

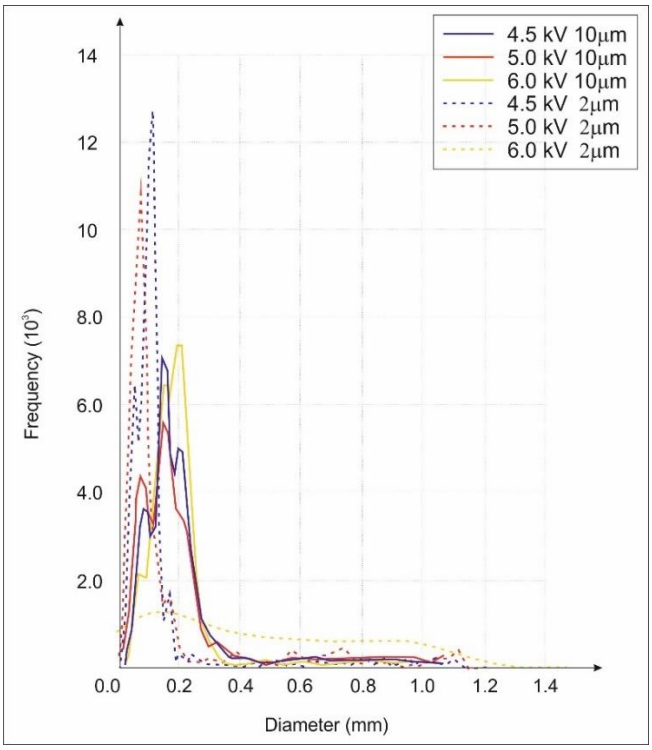

Figure 17: Droplet population generated with liquid T1F after 10µm and 2µm filters. The results are presented for three potentials (4.5, 5.0 and 6.0 kV) which represent intermittent mode with straight breakup (4.5 and 5.0 kV) and with lateral breakup (6.0kV). The solid lines represent the populations generated with the liquid after 10µm filter and the dashed lines represent the population generated after the 2µm filter.

From figure 17 is possible to see that the histogram curves of the populations produced with the smaller filter porous (2um) are shifted to the left for all tested potentials. Which is an indication that the application of the filter causes a general impact in the droplet size. The causes, even though not specifically studied, can be the relation between the nanoparticles and the liquid itself which can both impact how the electric charge is distributed in the liquid as well as the breakup mechanism itself. More studies have to be conducted to plausibly define the reasons for the observed impact. Additionally, it can be seen that the type of filter also impacted the total droplet production ratio, i.e. smaller filters' populations present higher peaks. Such impact is also expected if considered the volume fraction is highly impacted by the diameter which impacts the population frequency. Even though not always present, the trend presented here was also observed in other flows and other fluids. A more complete representation of the droplet population for the tested fluids and flows/potentials are represented in annex III, and a separate folder- population distribution.

3.1.4.3 – Influence of the tested fluid, filter and flow on droplet mode

To evaluate which sizes are the most produced sizes and how it is influenced by the applied filter, flow rate and type of fluid the below presented plot (figure 18) can be evaluated.

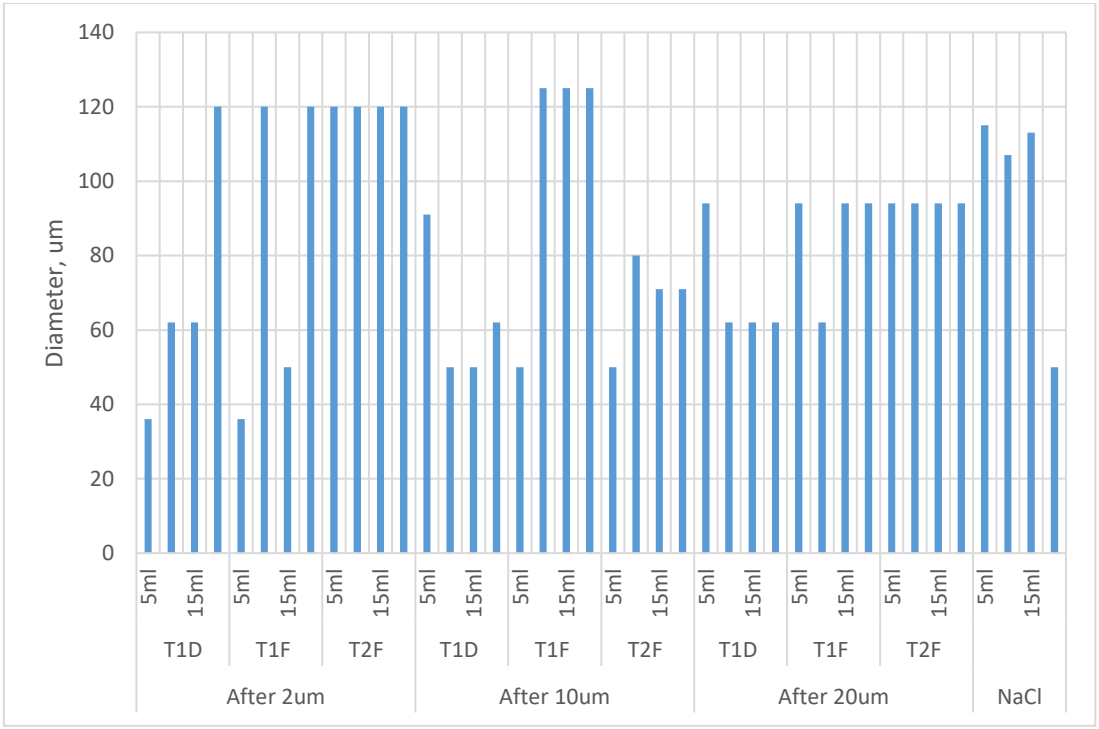

Figure 18: Population mode for different flow rate, different filter and different fluids (including NaCl solution). All the results are presented for an electric potential of approximately 4.5kV which is the potential when the spray changes between enhanced dripping into intermittent dripping mode (thus, with straight breakup).

As it can be seen in figure 18 the most produced droplet size (population mode) does not present straight forward trends. Some conclusions can be, nevertheless, inferred from the plot, namely: (i) T2 consistently produces mode values around the 100µm size. (ii) T1D produces the smaller modes of all fluids. (iii) there is no consistent effect caused by the used filter on the population mode.

The data also show that the produced droplet size ranges between 50 and 200µm, meaning, between the reported size encountered in the literature. However, when considered the data presented in figure 16, it is possible to see that EHDA can still produce droplets in the smallest expected size with the tested solution. The question is only whether such condition would be ideal considering the robustness of the system, i.e. smaller nozzles are more prone to clog, and instabilities, i.e. high potentials cause more instability and increase the chances for sparks episodes. An evaluation should be, thus, done buy the company regarding whether it is prudent to increase clogging chances in detriment of generating smaller droplet size.

3.1.4.4 – Estimation of Droplet Charge

Figure 19, presented in sequence, shows the calculated droplet charge for the experiments done with T1F before and after filtration. As expected, the bigger the diameter the more charge the droplet might accumulate. The plot also shows a slight smaller charge level for the droplets produced after 10µm filtration. This trend was not observed in the other tested liquids. The charge level, as it can be seen in the plot, is between 10^{-10} and 10^{-14} Coulombs per droplet. Agostinho (2013), when performing experiments with deionized water in the intermittent cone-jet mode, found droplet charges of 10^{-14}C as well, for droplets of 20-80µm.

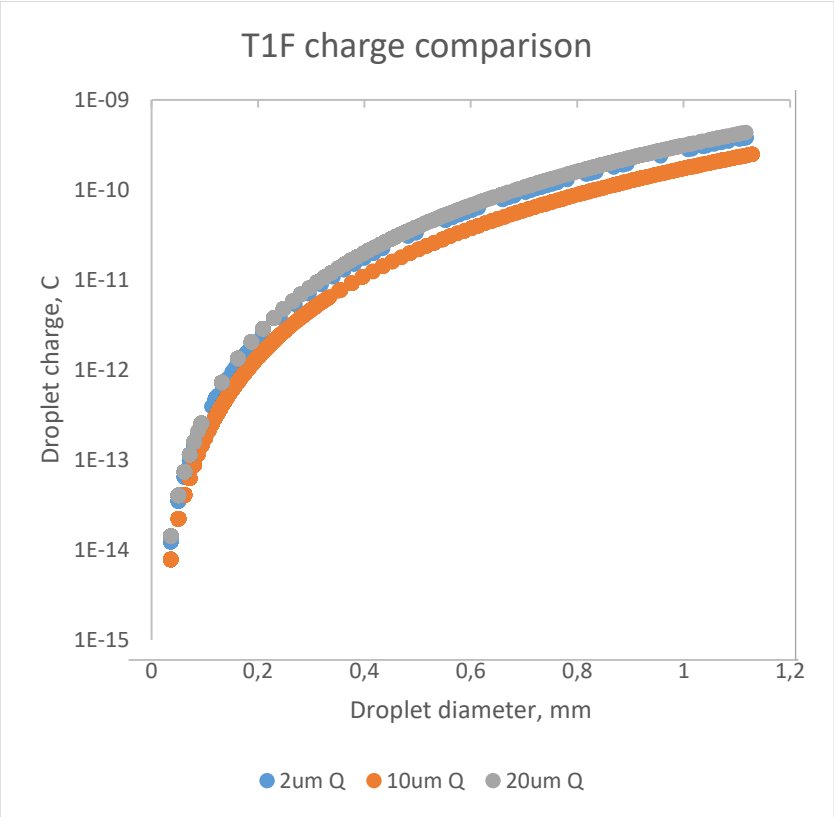

Figure 19: Droplet charge versus droplet diameter calculated for T1F before and after filtration.

It has also to be observed that the charge a droplet carries in electrospray will be concentrated on the droplet surface (Gauss Law) and that the total concentrated amount is dictated by the relation between the liquid surface tension and the columbic forces between the charges to hold the droplet intact, i.e. the Rayleigh effect. This relation (or, limit, if one will) is known as the maximum charge a droplet can hold before disrupting due to Coulombic fission and it is calculated as $R = 8 \cdot \pi (\gamma \cdot \varepsilon \cdot r_d^3)^{1/2}$. Where R is the Rayleigh limit, γ is the liquid surface tension, ε is the liquid permittivity and r_d the droplet radius. When observed the data presented in table 1, it is possible to see that both T1 and T2 have slightly smaller surface tension than water, but much higher relative permittivity, which indicates such liquids would be able to hold slightly more surface charge then water (electrosprayed) droplets. Even though this discussion is applied only to the Rayleigh limit of the droplets, it is also an indication that the studied liquid surface tension and permittivity properties would facilitate accumulation of surface charge, when compared to water/salt water liquids. And, therefore, provide better conditions for charge accumulation on droplets surface. This finding corroborates the results presented and discussed for figure 8 (relaxation time). Finally, the same droplet charge calculation was done as well for NaCl solution (figure 20) using similar flows and electric field intensity. As it can be seen, for this solution, droplets with the same diameter indeed are predicted to carry less charge. It is important to observe, nevertheless, that the droplet charge calculation conducted in this work is an approximation. Done by dividing the measured electric current values by the total amount of droplets produced during the same interval. Such method, even though largely used in EHDA research, is not the most precise one. More experiments should be conducted with higher precision equipment, e.g. Faraday cage, to provide better input on this specific aspect.

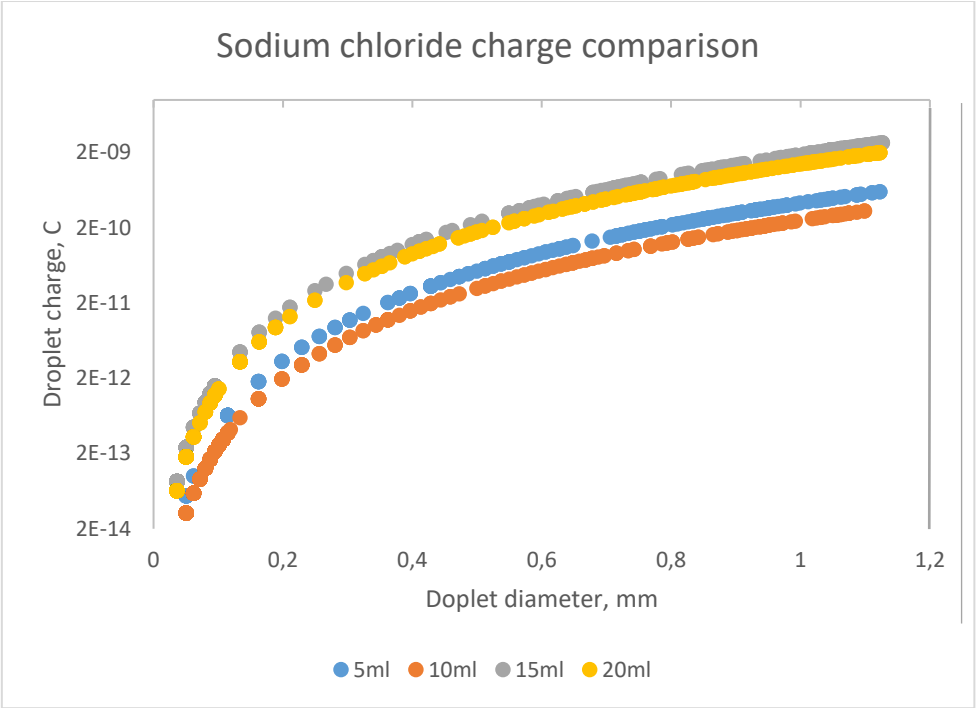

Figure 20: Droplet charge versus droplet diameter calculated for NaCl at different potentials.

4 Conclusions

The presented results can be summarized as follows:

- The physical chemical analysis indicated low to no influence of the particles on the liquid's density, dynamic viscosity and surface tension.
- High values obtained in the primitivity tests both for T1 and T2, for high frequencies, when compared to water, indicate the presence molecule's clusters bigger than water.
- The similar permittivity values found when comparing the substances, at the same frequency, with the NaCl solution, indicate the substances (and NaCl) create molecule's clusters with similar structures. At the same time, the higher conductivity indicates that T1 and T2 would provide faster ion mobility.
- More investigations have to be conducted to verify the reason for negative real permittivity coefficients, at high frequencies (above 1MHz), found for T1 samples.
- The combined influence of the particles on permittivity and conductivity created solutions with low electric relaxation time. Which indicates better tendency (when compared to water) to hold charge after atomization.
- ICP results show the presence of Ni and Fe is more pronounced than Al and Cr. Values encountered are below 1ppm for all tested elements.
- Bacteriologic analysis indicated low formation of colonies under the evaluated (reported) conditions.
- The physical-chemical properties of the liquids (especially surface tension and conductivity) did not allow the establishment of a cone-jet mode. Which basically indicate the droplet size will be still (strongly) affected by the nozzles size.
- The tested EHDA modes, i.e. intermittent cone-jet mode and micro-dripping, indicated high droplets dispersion, i.e. characteristically present in intermittent modes. Mode size was around 100µm but variable according to samples tested and used filter.

- With a smaller nozzle (ID=100µm) and higher potentials (around 12kV) average droplet size below 25µm could be achieved. However, for normal air conditions, such potential (using the 2cm distance between the electrodes) is highly unstable.
- Droplet charge analysis indicated higher surface charge for the tested liquids, even when compared to the sodium chloride solutions. Results also corroborates with the lower relaxation time found from the physical-chemical analysis.

References

Agostinho, L. L., E. A. van Os, T. Riemersma, M. Nederlof, and M. van der Staaij (2014). *Verbetering spuittechniek in de teelt van potgrond : proof of principle toepassing Electrospray in de Glastuinbouw*. (Rapport / Wageningen UR Glastuinbouw; No. 1322). Wageningen: Wageningen UR Glastuinbouw.

Agostinho, L.L.F, C.U. Yurteri, E.C. Fuchs and J.C.M. Marijnissen. Monodisperse water microdroplets generated by electrohydrodynamic atomization in the simple-jet mode. Appl. Phys. Lett. 100, 44105 (2012); doi: 10.1063/1.4729021

Agostinho, L.L.F, C.U. Yurteri, J. Wartena , S.P. Brouwer, E.C. Fuchs and J.C.M. Marijnissen. *Insulated multinozzle system for electrohydrodynamic atomization in the simple-jet mode*. Applied Physics Letters 2013, **102**, 194103.

Ashgriz, N. (2011). Handbook of atomization and sprays - theory and applications. New York:Springer science.

Avulapati, M. (2016). Puffing and micro-explosion of diesel–biodiesel–ethanol blends. *Fuels*, 59-66.

Bassiony M, A., Ibrahim A and El-Kassaby M. M, 2016. *An experimental study on the effect of using gas-to –liquid (GTL) fuel on diesel engine performance and emissions*. Alexandria Engineering Journal Vol 55 pp 2115-2124

Ballester, J.M., N. Fueyo, and C. Dopazo*. Combustion characteristics of heavy oil-water emulsions.* Fuel 1996; **75**, p 695-705

Bos, B. *Producing water-in-diesel emulsions with electrohydrodynamic atomization. A practical study about spray characteristics and stability.* Poster presented during the Wetsus Congress 2017.

Castillo-Orozco, E., A. Kar, and R. Kumar. *Electrospray mode transition of microdroplets with semiconductor nanoparticle suspension.* Scientific Reports 2017, article 5144.

Chelemuge, N. Tomoaki, Y. Kunio, T. Masanori, F. Koichi. *Commercial-scale demonstration of pollutant emission reduction and energy saving for industrial boilers by employing water/oil emulsified fuel.* Applied Energy (2012), **93(C)**, p 517-522.

Cherpak, N. T., Barannik, A. A., Prokopenko, Y. V., Smirnova, T. A., Filipov, Y. F. On the negative value of dielectric permittivity of the water surface layer. Applied Physics Letter (2003). Vol. 82 Number 22.

Gaveau A., Coetsier C., Roques C, Bacchin P., Dague E. et al. Bacteria transfer by deformation through microfiltration membrane. Journal of Membrane Science, Elsevier, 2017, 523, p 446-455.

Grace, J.M., and J.C.M. Marijnissen. *A review of liquid atomization by electrical means*. Journal of Aerosol Science 1994, **25**, p 1005-1019

Guru, M., U. Karakaya, D. Altiparmak, and A. Alicilar. *Improvement of diésel fuel properties by using additives.* Energy conversión and management, 2002. **43**, P 1021-1025

Hartman, R. Electrohydrodynamic atomization in the cone-jet mode, from physical modeling to powder production. 1998. PhD Thesis. TU Delft repository.

Hasegawa, H.; Naganuma, K.; Nakagawa, Y.; Matsuyama, T.; Membrane filter (pore size, 0.22–0.45 µm; thickness, 150 µm) passing-through activity of *Pseudomonas aeruginosa* and other bacterial species with indigenous infiltration ability. *FEMS Microbiology Letters*, Volume 223, Issue 1, June 2003, Pages 41–46, https://doi.org/10.1016/S0378-1097(03)00327-6.

Hansen, J., D. Johnson, A. Lacis, S. Lebedeff, P. Lee, D. Rind, and G. Russell. (1981). *Climate impact of increasing atmospheric carbon dioxide*. Science 1981, **213**, p 957-966.

Huo, M. (2014). Study on the spray and combustion characteristics of water–emulsified diesel. Fuel, 218-229.

Ilyas S.U., Pendyala R. and Marneni N. Preparation, sedimentation and agglomeration of nanofluids. Chemical Engineering Technology, 2014, 37 No. 12, p 2011-2021

Ilyas S.U., Pendyala R. and Marneni N. Stability and agglomeration of alumina nanoparticles in ethanol-watermixtures. 4th International Conference on Process Engineering and Advanced Materials

Khan, M. Y. , Z. A. Abdul Karim, F.Y. Hagos, A.R.A. Aziz, and I.M. Tan. *Current Trends in Water-in-Diesel Emulsion as a Fuel*. The Scientific World Journal, 2014, Article ID 527472, 15 pages

Lenin A, M.R. Swaminathan, and G. Kumaresan. *Performance and emission characteristics of a DI diesel engine with a nanofuel additive.* Fuel, 2013, **109**, p 362-365

Li. S., Z. Zhuo, L. He, and X. Huang. *Atomization characteristics of nano-Al/ethanol nanofluid fuel in electrostatic field.* Fuel 2019, **236**, p 811-819.

Lif, A., K. Holmberg. *Water-in-diesel emulsions and related systems*. Advances in colloid and interface science, 2006, **231-9**, p 123–126

Mura, E. (2010). Effect of dispersed water droplet size microexplosion phenomenon for water in oil emulsion. *Atomization and Sprays*, 791-799.

Namioka, T. (2012). Commercial-scale demonstration of pollutant emission reduction and energy saving for industrial boilers by employing water/oil emulsified fuel. *Applied Energy*, 517-522.

Ogunkoya, D. (2015). Performance, combustion, and emissions in a diesel engine operated with fuel-in-water emulsions based on lignin. *Applied Energy*, 851-861.

Pareta, R. and M.J. Edirisinghe. *A novel method for the preparation of biodegradable microspheres for protein drug delivery.* Journal of the Royal Society Interface, 2006

Park S.W., S. Kim, and C.S. Lee. *Effect of mixing ratio of biodiesel on breakup mechanisms on monodispersed droplets*. Energy fuels, 2006, **20(4)**, p 1709-1715

Pollak, G. and Binghua C. Solute-Free Interfacial Zones in Polar Liquids. *J. Phys. Chem. B* 2010, 114, 16, 5371-5375

Sadri, B., S. Faraji, B.V. Hokmabad and E. Esmaelizadeh. *Electrospray characteristics of aqueous KCl solutions with various electrical conductivities*. Conference paper, 2012, ICLASS2012 at Heidelberg

Sawyer, J. S. *Man-made Carbon Dioxide and the "Greenhouse" Effect*. Nature International Journal of Science. Nature, 1972, **239**, p 23–26

Saxena, V.; Kumar, N.; Saxena, V.K.; A comprehensive review on combustion and stability aspects of metal nanoparticles and its additive effect on diesel and biodiesel fueled C.I. engines. Renewable and Sustainable Energy Reviews 70 (2017) 563–588.

Shinjo, J. (2014). Physics of puffing and microexplosion of emulsion fuel droplets. *Physics of Fluids*.

Sridhar, K., S. Zheng, Y. Zhu. *Fibre humidity sensors with high sensitivity and selectivity based on interior nanofilm coated photonic crystal fibre long-period grating.* Sensors and Actuators, B, Chemical, **176**, P 264-274.

Statistical report 2017. Fuels Europe-refining products for everyday life

Vellaiyan, S. and K.S. Amirthagadeswaran. *The role of water-in-diesel emulsion and its additives on diesel engine performance and emission levels: A retrospective review.* Alexandria Engineering Journal, 2016, **55(3)** ,p 2463-2472

Verbeek, R., R. T. M. Smokers, G. Kadijk, A. Hensema, G.L.M. Passier, E.L.M. Rabe, B. Kampman, I.J. Riemersma. *Impact of biofuels on air pollutant emissions from road vehicles*. TNO Science and Industry, 2008

Wu, Y., and R. Clark. *Electrohydrodynamic atomization: a versatile process for preparing materials for biomedical applications.* Journal of Biomaterials Science, Polymer Edition, 2008, **19(5),** Nano-fiber Scaffold Science and Engineering

Xue, J., T.E. Grift, and A.C. Hansen. *Effect of biodiesel on engine performances and emissions.* Renewable and Sustainable Energy Reviews, 2011, **15**, p 1098-1116

Annex I – Potential windows tables

Potential window												
20 µm filtrate												
	T1D				**T1F**				**T2**			
Q, ml/h	**5**	**10**	**15**	**20**	**5**	**10**	**15**	**20**	**5**	**10**	**15**	**20**
Dripping	0kV	0kV	0kV	0kV	0kV	0kV	0kV	0kV	0kV	0kV	0kV	0kV
Enhanced dripping	<4.7kV	<4.7kV	<4.7kV	<4.7kV	<4.7kV	<4.7kV	<4.7kV	<4.7kV	<3,8kV	<3,8kV	<3,8kV	<3,8kV
Intermittent cone jet (straight break up)	4.7-4.8kV	4.7-5,4kV	4.7-5,7kV	4.7-5,9kV	4,7-4,8kV	4,7-5,5kV	4,7-5,8kV	4,7-6,0kV	3,8-4,2kV	3,8-4,7kV	3,8-5,0kV	3,8-5,1kV
Intermittent cone jet (lateral break up)	>4.8kV	>5,4kV	>5,7kV	>5,9kV	>4,8kV	>5,5kV	>5,8kV	>6,0kV	>4,2kV	>4,7kV	>5,0kV	>5,1kV
10 µm filtrate												
	T1D				**T1F**				**T2**			
Q, ml/h	**5**	**10**	**15**	**20**	**5**	**10**	**15**	**20**	**5**	**10**	**15**	**20**
Dripping	0kV	0kV	0kV	0kV	0kV	0kV	0kV	0kV	0kV	0kV	0kV	0kV
Enhanced dripping	< 4.7kV	<4.8kV	<4.8kV	<4.8kV	<4.7kV	<4.8kV	<4.8kV	<4.8kV	<3,8kV	<3,7kV	<3,8kV	<3,8kV
Intermittent cone jet (straight break up)	4.7-4.9kV	4.7-5,7kV	4.7-5,9kV	4.7-6,1kV	4,7-4,8kV	4,8-5,8kV	4,8-5,9kV	4,8-6,0kV	3,8-4,4kV	3,7-5,0kV	3,8-5,0kV	3,8-5,2kV
Intermittent cone jet (lateral break up)	>4.9kV	>5,7kV	>5,9kV	>6,1kV	>4,8kV	>5,8kV	>5,9kV	>6,0kV	>4,4kV	>5,0kV	>5,0kV	>5,2kV
2 µm filtrate												
	T1D				**T1F**				**T2**			
Q, ml/h	**5**	**10**	**15**	**20**	**5**	**10**	**15**	**20**	**5**	**10**	**15**	**20**
Dripping	0kV	0kV	0kV	0kV	0kV	0kV	0kV	0kV	0kV	0kV	0kV	0kV
Enhanced dripping	< 4,8kV	<4.8kV	<4.9kV	<4.7kV	<4.8kV	<4.9kV	<4.9kV	<4.8kV	<3,8kV	<3,8kV	<3,8kV	<3,8kV
Intermittent cone jet (straight break up)	4.8-4,9kV	4.8-5,8kV	4.9-6,0kV	4.7-6,1kV	4,8-4,9kV	4,9-5,8kV	4,9-6,1kV	4,8-6,2kV	3,8-4,2kV	3,8-4,5kV	3,8-5,1kV	3,8-5,0kV
Intermittent cone jet (lateral break up)	> 4,9kV	>5,8kV	>6,0kV	>6,1kV	>4,9kV	>5,8kV	>6,1kV	>6,2kV	>4,2kV	>4,5kV	>5,1kV	>5,0kV

Annex II – Droplet population for the different fluids and filters

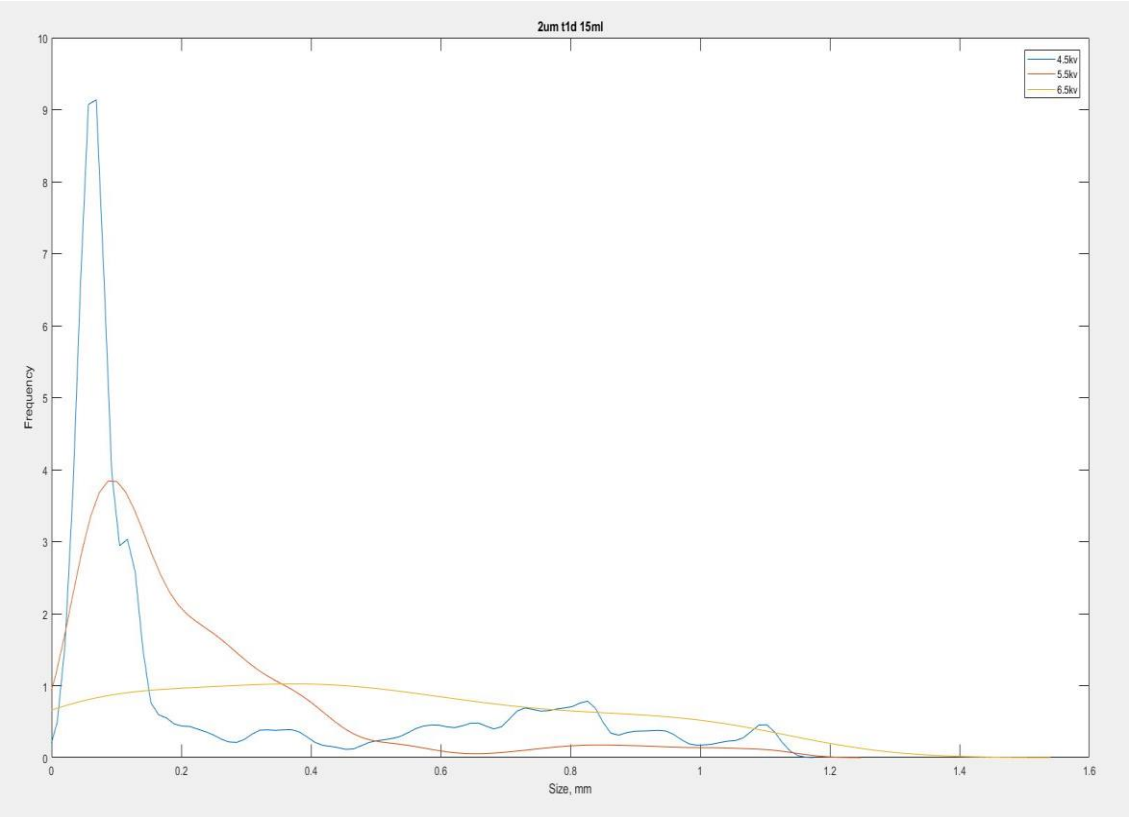

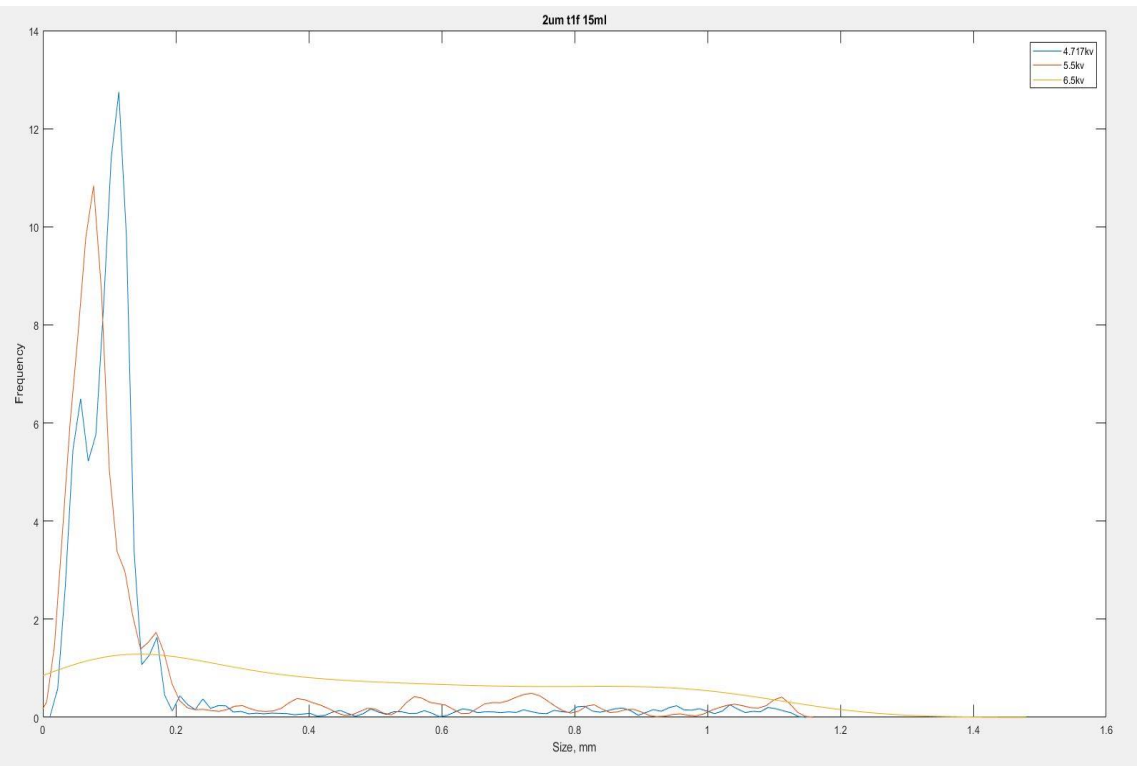

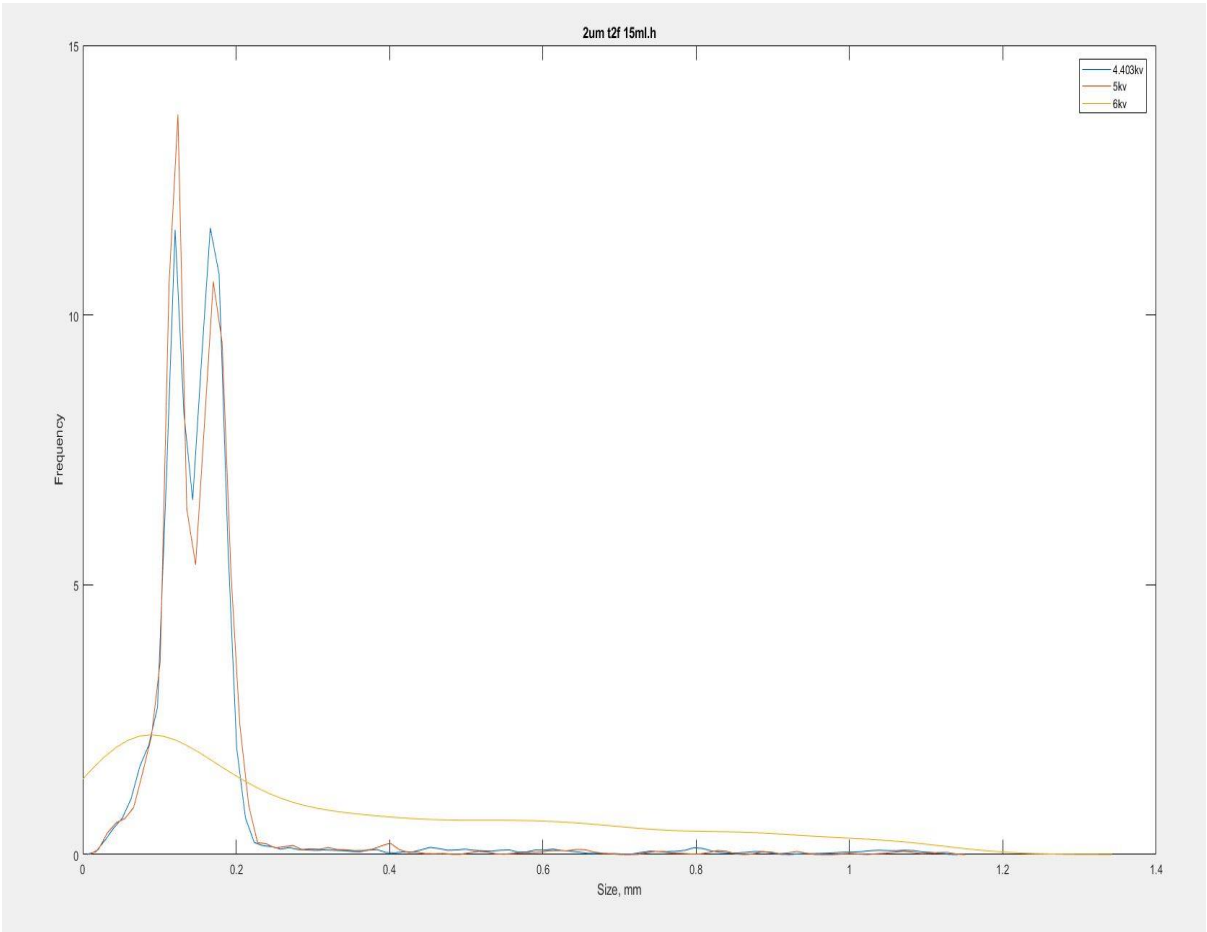
2um t2f 15ml.h
4.403kv
5kv
6kv
Frequency
Size, mm
0
5
10
15
0.2
0.4
0.6
0.8
1
1.2
1.4

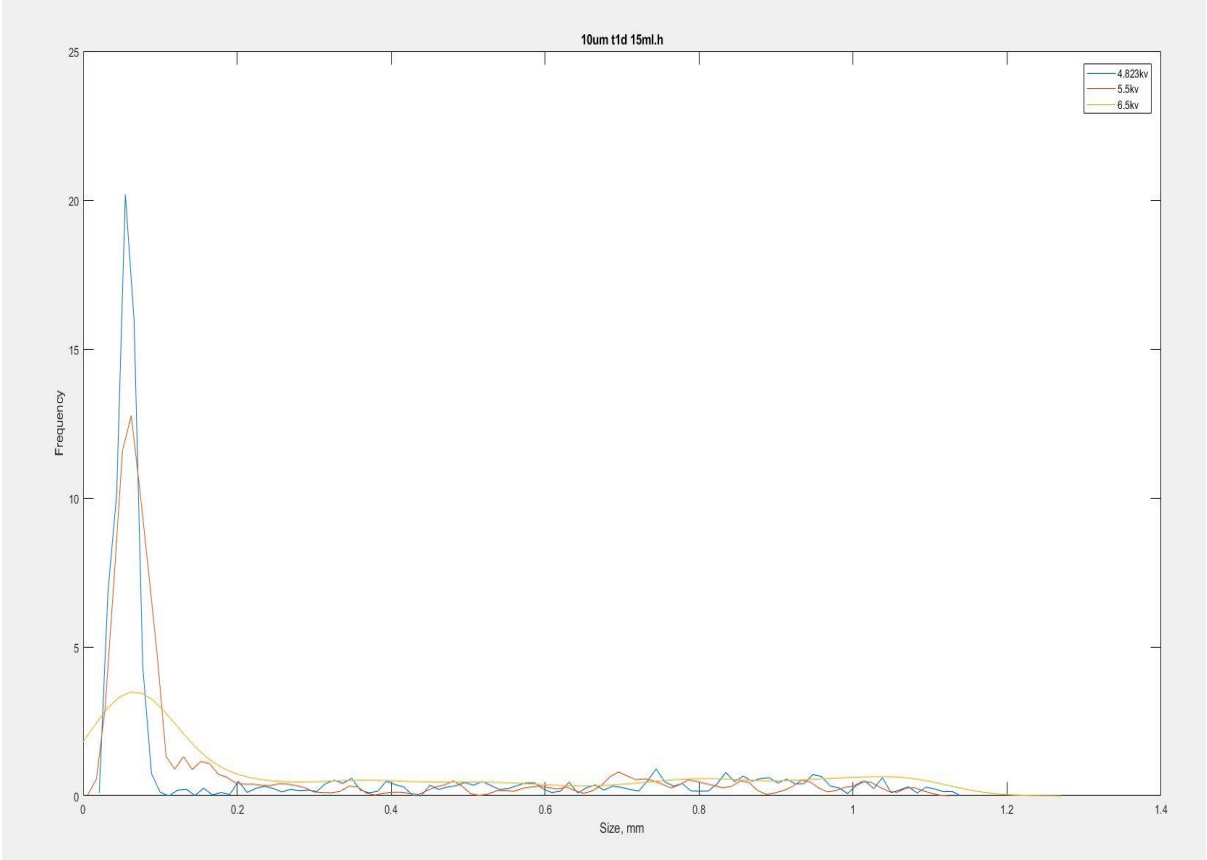
10um t1d 15ml.h
4.823kv
5.5kv
6.5kv
Frequency
Size, mm
0
5
10
15
20
25
0.2
0.4
0.6
0.8
1
1.2
1.4

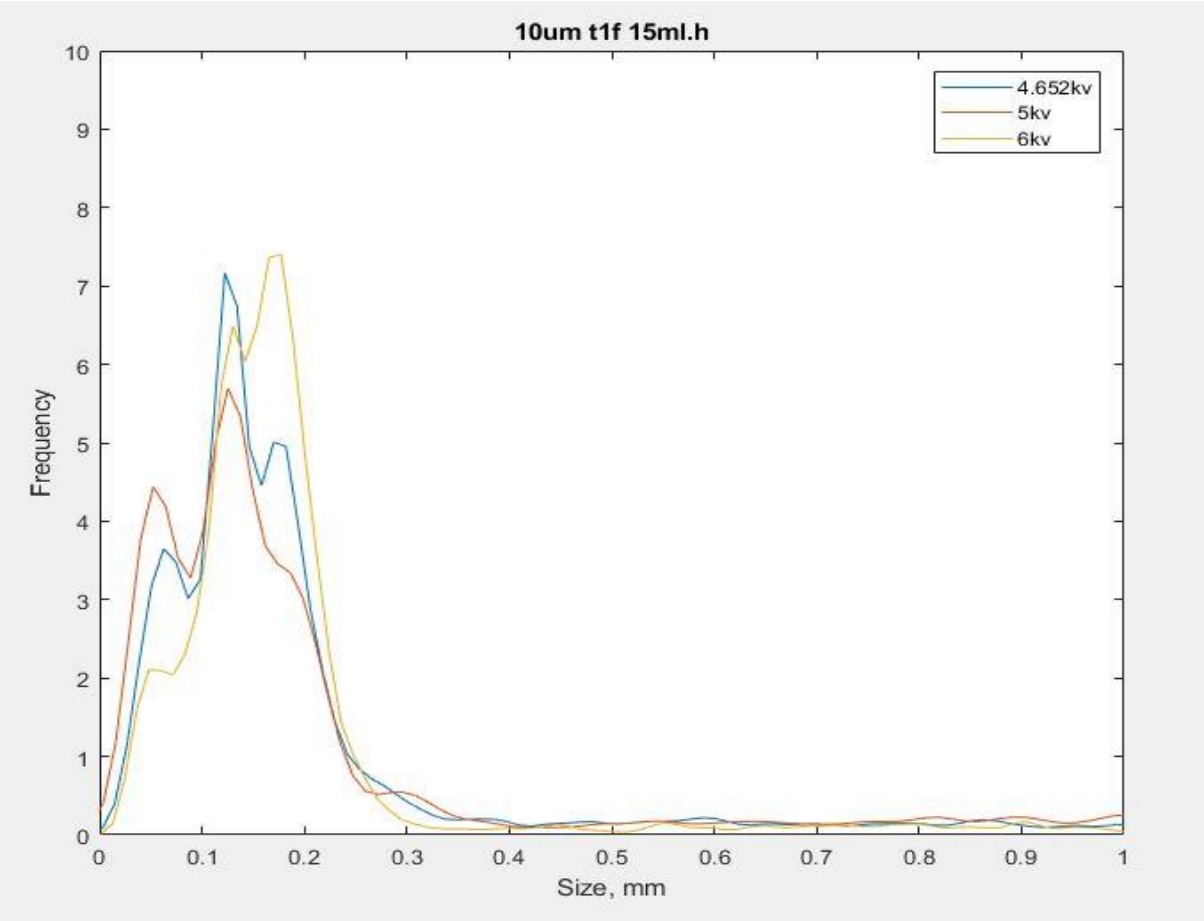
10um t1f 15ml.h
4.652kv
5kv
6kv
Frequency
Size, mm
0
1
2
3
4
5
6
7
8
9
10
0.1
0.2
0.3
0.4
0.5
0.6
0.7
0.8
0.9

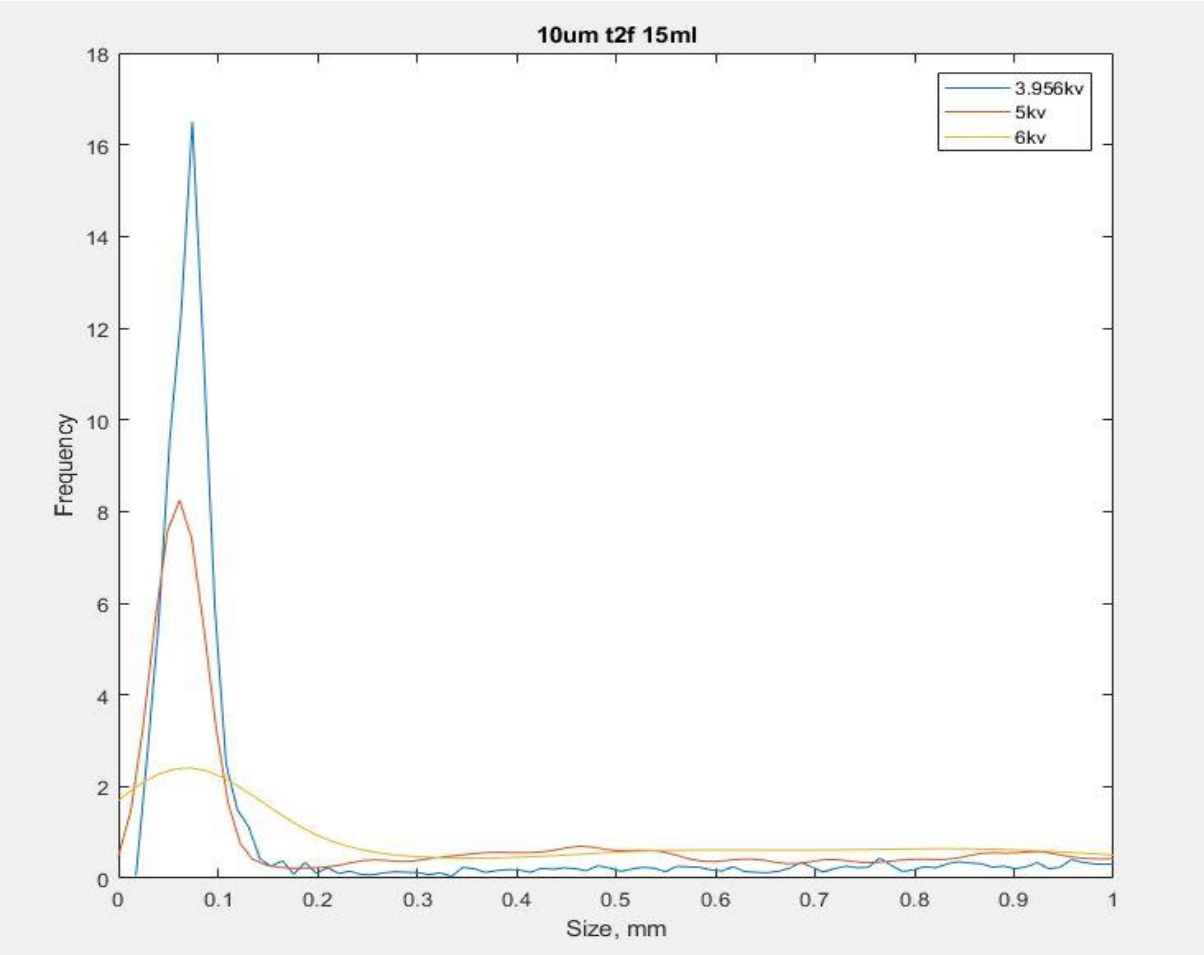
10um t2f 15ml
3.956kv
5kv
6kv
Frequency
Size, mm
0
2
4
6
8
10
12
14
16
18
0.1
0.2
0.3
0.4
0.5
0.6
0.7
0.8
0.9
1